

Super-resolution and denoising of fluid flow using physics-informed convolutional neural networks without high-resolution labels

Han Gao^a, Luning Sun^a, Jian-Xun Wang^{a,*}

^a*Department of Aerospace and Mechanical Engineering, University of Notre Dame, Notre Dame, IN*

Abstract

High-resolution (HR) information of fluid flows, although preferable, is usually less accessible due to limited computational or experimental resources. In many cases, fluid data are generally sparse, incomplete, and possibly noisy. How to enhance spatial resolution and decrease the noise level of flow data is essential and practically useful. Deep learning (DL) techniques have been demonstrated to be effective for super-resolution (SR) tasks, which, however, primarily rely on sufficient HR labels for training. In this work, we present a novel physics-informed DL-based SR solution using convolutional neural networks (CNN), which is able to produce HR flow fields from low-resolution (LR) inputs in high-dimensional parameter space. By leveraging the conservation laws and boundary conditions of fluid flows, the CNN-SR model is trained without any HR labels. Moreover, the proposed CNN-SR solution unifies the forward SR and inverse data assimilation for the scenarios where the physics is partially known, e.g., unknown boundary conditions. Several flow SR problems relevant to cardiovascular applications have been studied to demonstrate the proposed method's effectiveness and merit. Both Gaussian and non-Gaussian MRI noises are investigated to illustrate the denoising capability.

Keywords: Cardiovascular flows, PINN, Navier-Stokes, Field inversion, Surrogate modeling

*Corresponding author. Tel: +1 540 3156512

Email address: jwang33@nd.edu (Jian-Xun Wang)

1. Introduction

High-resolution (HR) information of fluid flow is critical for reliable qualitative and quantitative analyses for fluid systems in aerodynamics, mechanical, and biomedical engineering. Nonetheless, fluid flow data are often *sparse, incomplete, and noisy* in real-life scenarios due to the following reasons. First, flow data are typically spatiotemporal fields in large scales, which poses significant challenges to data analysis, sharing, and visualization due to limited storage space and large communication overhead. For example, the direct numerical simulation (DNS) of wall-bounded turbulent flows at Reynolds number of $Re_\tau = 10^4$ can generate more than 20 TB files at each time step, and the file size will increase exponentially as Re_τ grows [1]. Hence, scientists could only afford to store a small fraction of data (e.g., temporally sparse sequences, spatially downsampled volumes, or selective variable subsequences) for post hoc analysis. Second, the data resolution is often constrained by the ability of the measurement techniques. For example, flow magnetic resonance (MR) imaging has been widely used to quantitatively study cardiovascular blood flow dynamics [2, 3], but the spatial resolution and signal-to-noise ratio (SRN) of flow MR data are far from sufficient, limiting their clinical applications [4–6]. Therefore, it is significant and imperative to enhance the resolution and reduce the noise level, which is referred to as flow data *super-resolution and denoising*. Moreover, fluid flow data, even with high spatiotemporal resolutions, are usually sparse in the parameter space due to limited computational or experimental resources. For example, a single run of fully-resolved DNS of turbulent flows often takes days or weeks on high-performance computing facilities [1]. It becomes infeasible to perform massive queries in the parameter space to explore many different boundaries, geometries, and operational configurations for uncertainty quantification (UQ) and optimization. In such scenarios, data super-resolution in the parameter space can be treated as a cost-effective *surrogate model* that leverages the use of efficient low-resolution (LR) simulations or experiments. Scientists can opt to run their simulations or experiments at a low resolution and then upscale the results back to the target resolution, which will significantly save cost and speed up the process of scientific investigation and discovery.

Various efforts have been devoted to enhancing the spatial or/and temporal resolution of fluid flows. One type of approach focuses on extracting the coherent structures and correlation features from an existing HR database based on proper orthogonal decomposition (POD) [7–12], dynamic mode decomposition (DMD) [13, 14], or other sparsity-promoting representation techniques [15, 16]. However, these approaches are limited by the linearity assumption made for the reduced basis. The other types of super-resolution methods take advantage of the computational fluid dynamics (CFD) model to provide full-field predictions instead of learning from the offline database. The sparse LR data are fused into the CFD predictions using data assimilation (DA) techniques, e.g., ensemble Kalman filter, particle filters, or variational DA algorithms [17–23]. Nonetheless, physics-based CFD simulations are time-consuming in general, while the DA process usually involves numerous model evaluations, which could be computationally prohibitive.

The recent advances in machine learning (ML) and GPU computing open up a promising revenue to tackle this challenge. In past a few years, ML has been successfully applied in fluid dynamics [24, 25], for, e.g., turbulence closure modeling [26–30], inflow turbulence generation [31, 32], and fluid surrogate/reduced-order modeling [33–35], etc. In particular, the growing success of deep learning (DL)-based image super-resolution [36] in computer vision inspires the application of deep neural networks (DNN) for the flow field super-resolution and reconstruction [37–45]. Fukami et al. [37–39] applied the convolutional neural network (CNN) and hybrid downsampled skip-connection multiscale (DSC/MC) models for super-resolving downsampled HR data of both laminar and turbulent flows. To achieve a similar goal, Deng et al. [41] applied generative adversarial networks (GAN), while Liu et al. [46] adopted multiple temporal paths convolutional neural network (MTPC). Thuerey and co-workers designed a more complicated GAN architecture by considering temporal coherence to up-sample 3-D volumetric turbulent smoke data [45], and they further improved the scalability by decomposing the learning problem into multiple smaller sub-problems [47]. Bai et al [43] used a dictionary learning strategy to super-resolve turbulent smoke flows in a variety of animation context. Guo et al. [48] designed DL-based spatial upscaling solutions of vec-

tor fields for visualization purposes. Considering multi-scale features in fluid dynamics, Liu et al. [40] proposed a multi-resolution convolutional autoencoder (MrCAE) super-resolution architecture to dynamically capture different scaled flow features at different depths of the network, where the multi-grid method and transfer learning techniques are leveraged. Instead of using deep networks, Erichson et al. [49] proposed to directly capture an end-to-end mapping between the sparse measurements and the HR flow field using a shallow network. In the context of biomedical imaging, Ferdian et al. [50] developed a DL model for 4D flow MRI super-resolution, where CFD simulation data are utilized as HR labels for training.

Despite the great promise, the success of these DL models mainly relies on a large amount of offline HR data as labels, which are inaccessible in many cases, e.g., super-resolution of 4D flow MR images. Moreover, these recent data-driven upsampling approaches add visual complexity to an LR input but cannot guarantee that the super-resolved fields are faithful to the physical laws and principles. A more promising strategy is to incorporate prior physics knowledge into deep learning models to alleviate data requirements and improve learning performance. This idea of physics-informed deep learning has been recently explored for solving forward and inverse PDEs [51, 52], surrogate modeling [33, 53–55], and equation discovery [56–59]. For flow reconstruction and super-resolution, the divergence-free constraint for incompressible flow is the most straightforward one to be imposed on the learned solution, which can be done in a hard manner by either introducing stream functions or using spectral methods [42, 60–62]. Jiang et al. [60] proposed a MeshfreeFlowNet for super-resolving of LR solution fields of Rayleigh–Benard convection equations, where the training is regularized by the governing PDEs. In a similar vein, Subramaniam et al. [63] utilized the mass and momentum conservation law to constrain the training of a GAN for turbulence enrichment. Sun and Wang [64] developed a Bayesian physics-informed neural network using Navier-Stokes constrained Stein variational gradient descent to reconstruct fluid flows from limited noisy measurements. These studies have demonstrated the merits of introducing physics constraints. However, technical challenges remain in developing effective physics-informed DL models for super-resolution, especially for irregular domain problems in label-scarce or

label-free scenarios. In this work, we developed a physics-informed deep learning framework for super-resolving and denoising LR noisy flow fields with irregular geometries, where the HR data (labels) are not required. The novel contributions of this paper are summarized as follows: (a) we explored a deep learning solution for flow super-resolution without relying on HR data for training given well-posed physics; (b) the proposed method can simultaneously infer unknown conditions if the physics is partially known (e.g., boundary conditions is unknown); (c) we demonstrated the effectiveness of the proposed method on several fluid problems with irregular geometries and non-Gaussian noises in high-dimensional parameter space. The rest of the paper is organized as follows. The methodology of the proposed method is introduced in Section 2. Numerical results of several test cases, including vascular flow governed with known, unknown, and parametric boundary conditions, are presented in Section 3. To illustrate the model’s denoising capability, both Gaussian and Non-Gaussian noises (e.g., MRI noise) are studied. Finally, Section 4 concludes the paper.

2. Methodology

2.1. Overview

This work aims to reconstruct a high-resolution flow field from the corresponding low-resolution (possibly noisy) data obtained either by the low-fidelity simulations or measurements. Mathematically, this process can be described by the following mapping,

$$\mathcal{S} : (\hat{\Psi}^l; \mu) \mapsto (\hat{\Psi}^h; \mu), \quad (1)$$

where $\hat{\Psi}^l$ denotes the low-resolution (LR) noisy velocity field on a coarse mesh (e.g., 4D flow MRI measurements), and $\hat{\Psi}^h$ denotes the high-resolution (HR) noise-free flow field; μ represents the vector of physical parameters (e.g., geometry, inflow/outflow boundary conditions, and flow properties). In general, the dimension of $\hat{\Psi}^h$ is much higher than that of $\hat{\Psi}^l$ and thus could reveal more details of the flow field. We aim to develop a deep learning (DL) based super-resolution (SR) solution, where a CNN model \mathcal{S}^c is trained to approximate this LR-to-HR mapping as $\mathcal{S} \approx \mathcal{S}^c$. Once fully trained, the CNN model can be used to

super-resolve any given LR data and generate the corresponding HR noise-reduced flow solutions. In contrast to the previous works, the proposed SR-CNN will be trained purely based on physical laws with strictly imposed boundary conditions and thus does not need any HR data (i.e., labels). Moreover, the proposed learning framework is able to assimilate sparse observation data, unifying the forward and inverse modeling processes. Namely, when the underlying physics are partially known (e.g., boundary condition or other physical parameters are unknown), extra observations can be assimilated to enable forward super-resolution and inverse determination of unknowns simultaneously. The overall schematic of

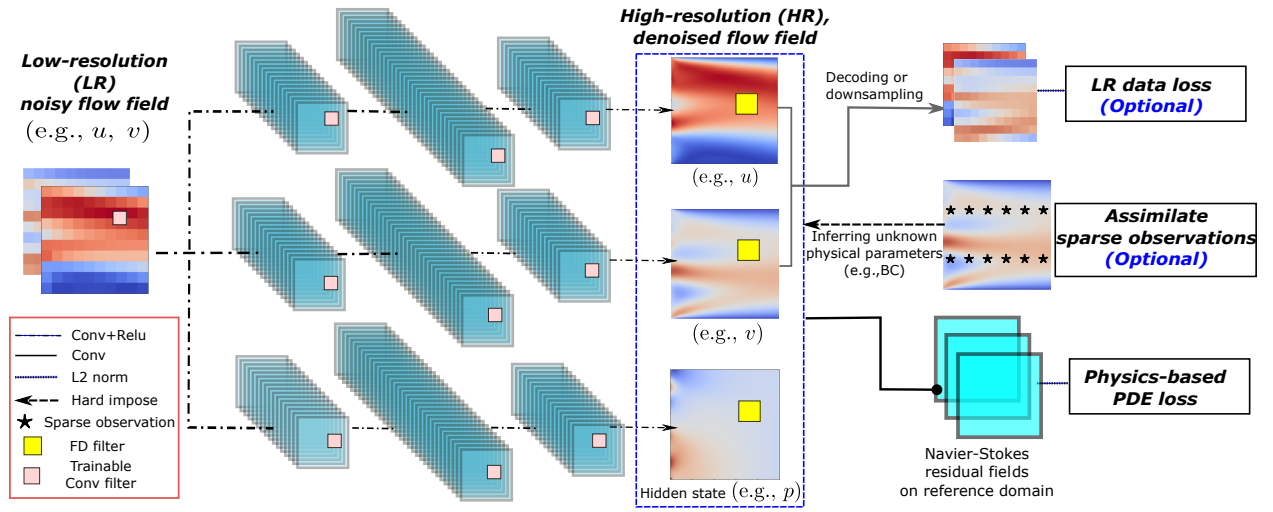


Figure 1: The schematic of physics-informed CNN for flow super-resolution.

the proposed physics-informed DL strategy for flow super-resolution is shown in Fig. 1, and each component of the framework will be detailed in the following subsections.

2.2. Learning architecture for super-resolution

A composite DL architecture is constructed (Fig. 1), which takes the (possibly noisy) LR velocity fields as the input channels and produces HR flow solutions. Separate sub-CNN is designed to capture each solution field individually, and thus the trainable network parameters are decoupled for different state variables with different magnitudes. This composite learning structure with decoupled sub-nets has been demonstrated effective in enhancing the learning performance for multivariate regression problems [48, 65, 66]. The composite

DL model consists of several convolutional decoders. Each of them has an identical structure of three hidden convolution layers, which is a classic CNN structure for single image super-resolution (SISR) [67]. Specifically, the input layer is first up-sampled to the target resolution using the bicubic interpolation and then goes through three convolution layers with trainable filters of size 5×5 , where 2D convolution operations with the padding of 2 and stride of 1 are applied. All the sub-nets are trained simultaneously with a unified physics-informed loss function as detailed in Section 2.3. The trainable parameters of the network are initialized from a uniform distribution of $\mathcal{U}\left(-\sqrt{\frac{1}{25C_{in}}}, \sqrt{\frac{1}{25C_{in}}}\right)$, where C_{in} is number of input channels. The network’s hyper-parameters are summarized in Table 1.

learning rate	# of hidden layers	# of hidden channels	Optimizer
10^{-3}	3	[16,32,16]	Adam[68]
padding size	strides	kernel size	Non-lienarity
2	1	5×5	ReLU[69]

Table 1: Hyper-parameters of the sub-CNN.

2.3. Physics-informed training

The composite network \mathcal{S}^c needs to be trained in order to approximate the LR-to-HR mapping \mathcal{S} as,

$$\hat{\Psi}^h = \mathcal{S}(\hat{\Psi}^l) \approx \mathcal{S}^c(\hat{\Psi}^l; \mathbf{W}^c), \quad (2)$$

which is an optimization problem traditionally solved based on a large amount of labeled data. Namely, when a set of n_d^h LR/HR data pairs $\{\hat{\Psi}_i^l, \hat{\Psi}_i^h\}_{i=1}^{n_d^h}$ are available, the network trainable parameters \mathbf{W}^c can be optimized by iteratively minimizing the mismatch between the CNN predictions $\mathcal{S}^c(\hat{\Psi}_i^l)$ and the HR labels $\hat{\Psi}_i^h$ as follows,

$$\tilde{\mathbf{W}}^c = \arg \min_{\mathbf{W}^c} \underbrace{\sum_{i=1}^{n_d^h} \left\| \mathcal{S}^c(\hat{\Psi}_i^l; \mathbf{W}^c) - \hat{\Psi}_i^h \right\|_{\Omega_p}}_{\text{data-based loss: } \mathcal{L}^d}, \quad (3)$$

where $\|\cdot\|_{\Omega}$ denotes the L_2 norm over the entire domain Ω_p . However, this *data-driven* training process requires enormous labeled data (i.e., HR samples), which are usually less

accessible and way more expensive to acquire than the input data (i.e., LR samples). In many cases, the HR labels are even not available at all due to the resolution limit of the measurement techniques. In this work, we try to tackle this challenge and develop a CNN-SR solution *without relying on HR data* as training labels. A physics-informed learning strategy is adopted to enable label-free training in data-sparse/absent scenarios. The general idea is to leverage the (partially) known physics of the fluid flow (e.g., conservation laws and boundary conditions) to drive the CNN training such that the super-resolved flow information is learned from the flow governing equations instead of massive HR labels. Here we consider fluid problems governed by the steady incompressible Navier-Stokes equations parameterized by $\boldsymbol{\mu}$,

$$\mathcal{R}(\mathbf{u}, p; \boldsymbol{\mu}) = \mathbf{0} := \begin{cases} \nabla \cdot \mathbf{u} = \mathbf{0}, & \text{in } \Omega_p, \\ (\mathbf{u} \cdot \nabla) \mathbf{u} + \frac{1}{\rho} \nabla p - \nu \nabla^2 \mathbf{u} + \mathbf{b}_f = \mathbf{0}, & \text{in } \Omega_p, \end{cases} \quad (4)$$

where \mathbf{u} is the velocity and p is the pressure; ν and \mathbf{b}_f represents the viscosity and body force of the fluid flow, respectively. The flow solutions can be uniquely determined with given boundary condition (BC), $\mathcal{B}(\mathbf{u}, p; \boldsymbol{\mu}) = 0$, on $\partial\Omega_p$. Since the CNN super-resolved flow fields should satisfy the governing equations, the training can be recast as a constrained optimization problem by minimizing the PDE residuals,

$$\begin{aligned} \tilde{\mathbf{W}}^c &= \arg \min_{\mathbf{W}^c} \sum_{i=1}^{n_d} \underbrace{\left\| \mathcal{R} \left(\mathcal{S}^c(\hat{\boldsymbol{\Psi}}_i^l; \mathbf{W}^c) \right) \right\|_{\Omega_p}}_{\text{PDE-based loss: } \mathcal{L}^p}, \\ s.t. \quad &\mathcal{B} \left(\mathcal{S}^c(\hat{\boldsymbol{\Psi}}_i^l; \mathbf{W}^c); \boldsymbol{\mu} \right) = 0, \text{ on } \partial\Omega_p, \end{aligned} \quad (5)$$

where $\hat{\boldsymbol{\Psi}}_i^l = \mathbf{u}(\boldsymbol{\mathcal{X}}^l; \boldsymbol{\mu}_i)$ is the LR velocity field discretized on a coarse mesh $\boldsymbol{\mathcal{X}}^l$, and $\hat{\boldsymbol{\Psi}}_i^h = [\mathbf{u}(\boldsymbol{\mathcal{X}}^h; \boldsymbol{\mu}_i), p(\boldsymbol{\mathcal{X}}^h; \boldsymbol{\mu}_i)]^T \approx \mathcal{S}^c(\hat{\boldsymbol{\Psi}}_i^l; \mathbf{W}^c)$ is the CNN super-resolved flow fields on a fine mesh $\boldsymbol{\mathcal{X}}^h$. To evaluate the PDE residuals on the discretized domain, we use convolution operations with the finite difference filters to compute the derivative terms in Eq. 4, and the details are given in [Appendix A](#). The boundary condition is strictly enforced into the CNN architecture, where the boundary operator \mathcal{B} is discretized and imposed on the CNN-SR predictions in a hard manner using padding operations [66]. In contrast to the traditional label-based data-

driven approach, the number n_d^p of training samples is not constrained by the availability of HR data. Hence, the training space can be freely explored with a large number of LR data $\hat{\Psi}_i^l$, which are assumed to be very cheap to obtain. Moreover, to further facilitate the PDE-based training, the CNN-SR output can be down-sampled via the pooling operation or an extra encoder) to construct a *LR data loss*, the mismatch between LR input data and downsampled CNN-SR output predictions (as shown in Fig. 1). However, the LR-data loss should only be included if the LR data are noise-free; otherwise, the network may tend to overfit the data noise.

2.4. Assimilate sparse observation data for partially known physics

It is commonly known that the flow physics is governed by the Navier-Stokes equations $\mathcal{R}(\mathbf{u}, p; \boldsymbol{\mu}) = 0$, but some of the physical parameters $\boldsymbol{\mu}$, such as inlet profiles or fluid properties, are unknown in many cases. On the other hand, it is possible to access additional observation data, which, however, is often spatially sparse and/or indirect to the quantity of interest. For example, the 3D full-field velocity information is obtained using 4D flow MRI techniques in cardiovascular applications, but the spatial resolution and SNR are unsatisfied and need enhancement [4]. More accurate flow field data can be observed by 2D phase-contrast MR imaging, which is only available on a limited number of 2D slices. The proposed physics-informed CNN-SR framework can naturally leverage these additional sparse observations to enable both forward super-resolution and inverse parameter determination in a unified manner. Here we introduce a novel approach of assimilating additional sparse observation data to infer the under-determined physical conditions/parameters $\boldsymbol{\mu}^s \subset \boldsymbol{\mu}$. First, the unknowns (e.g., boundary conditions) are parameterized as a trainable vector $\boldsymbol{\mu}^s$, which are incorporated into the SR learning architecture either through the equation-based loss function or strictly-imposed boundary conditions. Second, the sparse observations \mathbf{Y}^{obs} are assimilated into the network in a hard manner, where the CNN-SR predictions are strictly enforced to be equal to the data at sparse locations by constructing the model output Ψ^c as,

$$\mathcal{F}^{s2o}(\Psi^c) = \mathcal{F}^{s2o}(\hat{\Psi}^c) \times 0 + \mathbf{Y}^{obs}, \quad (6)$$

where $\hat{\Psi}^c$ is the CNN-SR raw output and $\mathcal{F}^{s2o} : \Psi \rightarrow Y$ indicates the state-to-observable map. Therefore, the constrained optimization for PDE-driven training is recast as,

$$\begin{aligned} \tilde{W}^c, \mu = \arg \min_{W^c, \mu} \sum_{i=1}^{n_d} \underbrace{\left\| \mathcal{R} \left(\mathcal{S}^c(\hat{\Psi}_i^l; W^c); \mu \right) \right\|_{\Omega_p}}_{\text{PDE-based loss: } \mathcal{L}^p}, \\ \text{s.t. } \begin{cases} \mathcal{B} \left(\mathcal{S}^c(\hat{\Psi}_i^l; W^c); \mu \right) = 0, \text{ on } \partial\Omega_p, \\ \mathcal{F}^{s2o} \left(\mathcal{S}^c(\hat{\Psi}_i^l; W^c) \right) - Y^{obs} = 0, \end{cases} \end{aligned} \quad (7)$$

where both the network parameter vector \tilde{W}^c and physical parameter vector μ are inferred simultaneously. It worth mentioning that the proposed “hard” DA approach is based on the assumption that the observation data are relatively precise. When assimilating very noisy observations, the penalty-based “soft” approach used in the PINN [51] should be employed to avoid overfitting the data noise.

2.5. Coordinate transformation for irregular domain

A general limitation of CNNs is that they can only handle problems defined on rectangular domains with uniform grids since the convolution operations are originally designed for processing images described on uniform meshes. However, the geometries in most scientific applications are complex and irregular (e.g., subject-specific vessel geometries in cardiovascular applications). In order to perform physics-informed super-resolution on non-rectangular domains, we adopt the geometry-adaptive CNN formation proposed by Gao et al. [66], where the elliptic coordinate transformation is utilized to reformulate the PDE-constrained learning from the irregular physical domain ($\mathbf{x} \in \Omega_p$) to the regular reference domain ($\xi \in \Omega_r$). Particularly, the one-to-one coordinate transformation map $\mathcal{G} : \Omega_r \rightarrow \Omega_p$ is obtained numerically by solving an elliptic problem, e.g., diffusion equations. The Jacobians of the map \mathcal{G} are then computed to convert differential operators from the physical domain to the reference domain,

$$\frac{\partial}{\partial x} = \frac{1}{J} \left[\left(\frac{\partial}{\partial \xi} \right) \left(\frac{\partial y}{\partial \eta} \right) - \left(\frac{\partial}{\partial \eta} \right) \left(\frac{\partial y}{\partial \xi} \right) \right], \quad (8a)$$

$$\frac{\partial}{\partial y} = \frac{1}{J} \left[\left(\frac{\partial}{\partial \eta} \right) \left(\frac{\partial x}{\partial \xi} \right) - \left(\frac{\partial}{\partial \xi} \right) \left(\frac{\partial x}{\partial \eta} \right) \right], \quad (8b)$$

where coordinates of physical domain and reference domain are $\mathbf{x} = [x, y]^T$ and $\boldsymbol{\xi} = [\xi, \eta]^T$, respectively; $J = \frac{\partial x}{\partial \xi} \frac{\partial y}{\partial \eta} - \frac{\partial x}{\partial \eta} \frac{\partial y}{\partial \xi}$ is the determinant of the Jacobian matrix and metrics $\frac{\partial y}{\partial \eta}$, $\frac{\partial y}{\partial \xi}$, $\frac{\partial x}{\partial \eta}$, and $\frac{\partial x}{\partial \xi}$ can be precomputed and remain constant given \mathcal{G} . Using elliptic coordinate transformation, the PDE-based loss function is reformulated on the reference domain, and thus the classic CNN backbone can be directly used for irregular geometries. For more details, the reader is referred to [66].

3. Result

3.1. Overview

We demonstrate the physics-informed CNN-SR analysis on several internal flow cases relevant to cardiovascular applications. The LR input will be denoised and enhanced to the high-resolution field for both deterministic and parametric scenarios. We first study the flow field in a 2D vascular domain with a deterministic setting, where the governing PDEs and boundary conditions are well defined. Moreover, we also investigate the scenario that the flow physics is partially known, (e.g., the inlet boundary condition is unknown) to demonstrate the CNN-SR solution of unifying forward and inverse problems with additional observation data. Lastly, we present the parametric SR analysis for internal flows with a parameterized inlet velocity profile in a high-dimensional parameter space.

3.1.1. Synthesis of low-resolution, noisy data

Synthetic LR data are generated from finite volume (FV)-based CFD simulations on coarse meshes. The simulated LR velocity fields are corrupted by artificial measurement noises. Two types of noise models are considered: (1) Gaussian noise and (2) non-Gaussian flow MRI noise.

- **Gaussian noise model:** The LR velocity field $\boldsymbol{\Psi}^l$ is corrupted by an independent and identically distributed (i.i.d.) Gaussian noise factor $\boldsymbol{\epsilon} \sim \mathcal{N}(\mathbf{0}, \mathbf{I})$ as,

$$\hat{\boldsymbol{\Psi}}^l = \boldsymbol{\Psi}^l \cdot (\mathbf{I} + c\boldsymbol{\epsilon}), \quad (9)$$

where the parameter $c \in [0, 1]$ controls the noise level.

- **Non-Gaussian MRI noise model:** To mimic the LR data obtained from the flow MR imaging, the five-point balanced phase-contrast method [70] is employed to encode the CFD velocity field into the phase space by $\mathbf{S} = \mathcal{F}(\Psi^l)$, where \mathbf{S} is a complex matrix of five column vectors. Different levels of complex Gaussian noise are added to the complex data, and the synthetic noisy MR flow field can be then obtained via the inverse five-point map $\mathcal{F}^{-1}(\cdot)$ following the Ref of [4],

$$\begin{aligned}\hat{\mathbf{S}} &= \mathbf{S} + \frac{c}{\sqrt{2}} |\Psi^l| \cdot \mathbf{I}(\epsilon_1 + \epsilon_2 i), \\ \hat{\Psi}^l &= \mathcal{F}^{-1}(\hat{\mathbf{S}}),\end{aligned}\tag{10}$$

where i is the imaginary unit, $\epsilon_1, \epsilon_2 \stackrel{\text{i.i.d}}{\sim} \mathcal{N}(\mathbf{0}, \mathbf{I})$, and $c \in [0, 1]$ controls the noise level. The Gaussian noise imposed in the phase space will become highly non-Gaussian once being mapped back to the physical velocity space, For more details of the forward and inverse five-point maps $\mathcal{F}(\cdot)$ and $\mathcal{F}^{-1}(\cdot)$, we refer to the Refs of [4, 70].

3.1.2. Cases setup

To evaluate the CNN-SR performance, we generate high-resolution CFD data ($\hat{\Psi}^h$) as the reference. Moreover, the upsampled results from the bicubic interpolation will also be computed for comparison. Both the LR and HR CFD simulations are conducted using OpenFOAM [71], an open-source C++ library for FV simulations. The relative error metric e is defined as,

$$e = \sqrt{\frac{\|\hat{\Psi}^c - \hat{\Psi}^h\|_{L_2}}{\|\hat{\Psi}^h\|_{L_2}}}.\tag{11}$$

Specifically, the FV solutions of the steady incompressible Navier-Stokes equations are solved using the Semi-Implicit Method for Pressure Linked Equations (SIMPLE) algorithms [72], where the Rhie and Chow interpolation with collocated grids is adopted to prevent the pressure-velocity decoupling [73]. The nonlinear convection term is discretized based on the Gauss theorem with the second-order bounded linear upwind interpolation (i.e., Gauss linearUpwind Scheme in OpenFOAM), and the diffusion term is discretized using the central Gauss linear interpolation with the explicit non-orthogonal correction for surface normal

gradients (i.e., Gauss linear corrected). The physics-informed CNN-SR model is implemented in PyTorch [74], and training is conducted on an NVIDIA GeForce RTX 2080 Graphics Processing Unit (GPU) card. The training histories for all the test cases are summarized by Fig. C.11 in Appendix C. The code and datasets for this work will be available at <https://github.com/Jianxun-Wang/PICNNSR> upon publication.

3.2. Non-parametric super-resolution

The proposed physics-informed CNN-SR model is constructed to super-resolve the LR flow field in a non-parametric setting. Namely, the DL model is trained to learn the LR-to-HR map, $\mathcal{S} : (\hat{\Psi}^l; \mu) \mapsto (\hat{\Psi}^h; \mu)$, where the physical parameter μ is fixed. A 2D laminar flow with an irregular vascular geometry is investigated, as shown in Fig. 2. The flow starts at the bottom edge (i.e., inlet) and moves out at the upper edge (i.e., outlet), where the non-slip wall boundary condition is imposed on the left and right boundaries. The LR data

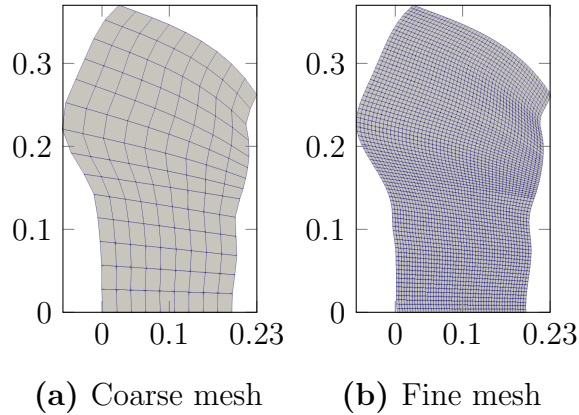


Figure 2: The low-resolution mesh (126 cells) and high-resolution mesh (3773 cells). The LR input data is refined by $30\times$

is obtained from a coarse mesh of 126 cells, while the HR target mesh has 3773 cells. The CNN-SR will take the LR data as the input and generates spatially refined data by $30\times$.

3.2.1. Known boundary condition

We first consider a deterministic scenario with well-posed physics, where both the governing PDEs (i.e., incompressible Navier-Stokes equations) and boundary conditions are well

defined. In particular, the inlet boundary condition is known as a constant profile $\mathbf{u} = [0, 1]$ and the outlet is defined by $\nabla \mathbf{u} \cdot \mathbf{n} = 0$ and $p = 0$, where \mathbf{n} is the local wall-normal vector. Figure 3 shows the CNN-SR velocity fields from the LR data with a 100% Gaussian noise ($c = 1.0$). Due to the mesh coarseness, the LR field presents a mosaic pattern and provides very limited information. The SR solution directly upscaled by the bicubic interpolation is unsatisfactory since the large Gaussian noise makes the bicubic-SR solution highly unphysical. In contrast, the CNN-SR solution well agrees with the HR reference data (truth). The flow details of the boundary layer and velocity development can be accurately captured, where the large Gaussian noises are significantly reduced. The relative error of the CNN-SR field is 0.067, which is an order lower than that of the bicubic-SR result (0.520).

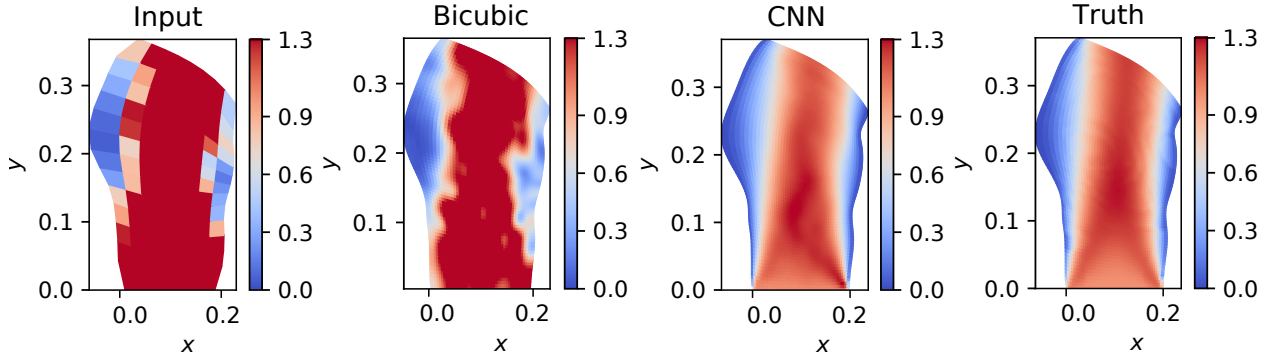


Figure 3: The super-resolved results of LR input with the 100% Gaussian noise ($c = 1.0$). The relative errors of the bicubic-SR and CNN-SR fields are 0.520 and 0.067, respectively.

For the experiment with artificial MRI noises shown in Fig. 4, the LR velocity field becomes even more unphysical and the flow information is overwhelmed by the large non-Gaussian MRI noises. Using bicubic interpolation does not show any improvement. Compared to the HR reference, the Bicubic-SR velocity field barely captures any flow physics and has a large relative error of 0.617. However, the CNN-SR model, informed by the Navier-Stokes equations, can largely remove the MRI noises and generate an accurate super-resolved velocity field with a relative error of 0.066. The encouraging results show great promise of the proposed method for enhancing the spatial resolution of 4D flow MR imaging, for which the HR labels are often unavailable.

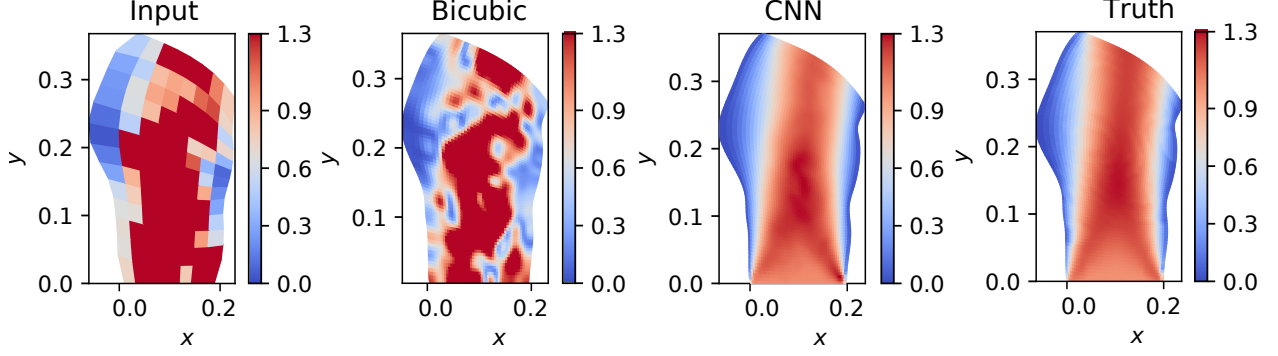


Figure 4: The super-resolved results of LR input with the 100% MRI noise ($c = 1.0$). The relative errors of bicubic-SR and CNN-SR fields are 0.617 and 0.066, respectively.

3.2.2. Unknown boundary condition

In this subsection, we demonstrate the capability of unifying the super-resolution and data assimilation for the situation where the physics is ill-posed (e.g., unknown boundary conditions), but additional sparse observation data is available. This scenario is quite common in cardiovascular applications. The 4D flow MR imaging techniques enable noninvasive and *in vivo* measurements of full-field blood flow information, whose spatial resolution, however, is too low to perform any quantitative analysis. Although the Navier-Stokes equations can be used to refine the LR data, the boundary conditions (e.g., inlet velocity field and outlet pressure distributions) are often not available in clinical practice. On the other hand, some sparse high-fidelity observations can be obtained by the 2D PC-MRI on a few 2D slices, which can be assimilated to infer the unknown boundaries. To mimic this scenario, we conduct a numerical experiment with the same setting as above, where the synthetic LR data corrupted by 100% MRI noises are super-resolved using the Navier-Stokes-informed CNN. In contrast to the previous example, we here assume the true inlet velocity profile $\mathbf{u} = [0, 100x(0.2 - x)]$ is unknown, but more accurate velocity observations are given only on four slices ($\sim 2\%$ of mesh grids), as an analogue of the sparse 2D PC-MRI data (see Fig. 5). It can be seen that not only the LR noisy flow field has been super-resolved to be in a good agreement with the HR reference ($e = 0.029$), but also the unknown inlet velocity profile (a 45-dimensional field) can be accurately recovered in a unified manner.

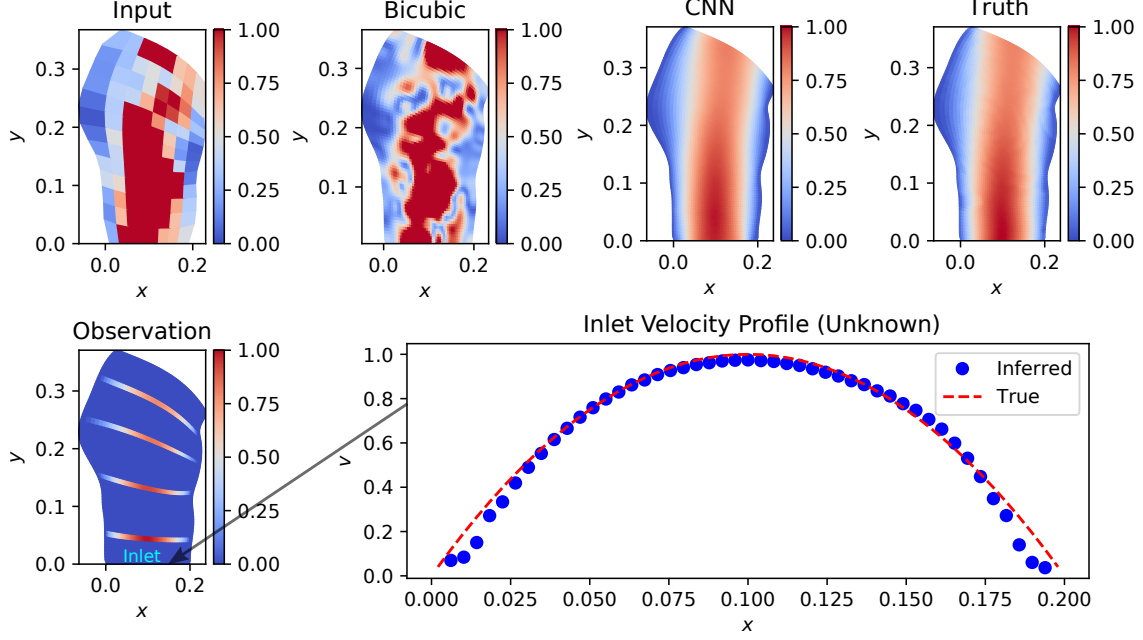


Figure 5: The super-resolved results of LR input with the 100% MRI noise ($c = 1.0$) where inlet boundary is unknown. The sparse velocity observations (on $\sim 2\%$ of mesh grids) are assimilated to infer the inlet velocity profile (a 45-dimensional field).

3.3. Parametric super-resolution

The proposed CNN-SR solution can be applied for flow super-resolution in the parametric setting, leveraging the powerful interpolatory capability of DL models in high-dimensional parameter space. Namely, the DL model is trained to capture the operator, $\mathcal{S} : (\hat{\Psi}^l; \mu) \mapsto (\hat{\Psi}^h; \mu)$, where the physical parameters μ could vary in a high-dimensional space. Once fully trained, the CNN-SR model can be treated as a cost-effective surrogate model that takes the LR data to produce HR solutions. Since the low-fidelity simulations or experiments are relatively cheap to conduct, the trained CNN-SR surrogate could significantly facilitate many query applications, e.g., uncertainty propagation, optimization, and sample-based Bayesian inference. To demonstrate parametric SR capability, we consider internal flows with spatially-varying inflow boundary conditions (including non-zero secondary flow). The CNN-SR is trained to refine the LR flow fields by $400\times$. As shown Fig. 6, the inlet velocity field $\mathbf{u}(\mathbf{x})$ is set on the left edge ($x = 0$), while the zero-pressure outlet is prescribed

on the right edge ($x = 1$). Both the top and bottom edges ($y = 0, y = 1$) are set as non-slip walls. Each component of the inlet velocity field ($\mathbf{u} = [u(\mathbf{x}), v(\mathbf{x})]^T$) is modeled by a scalar

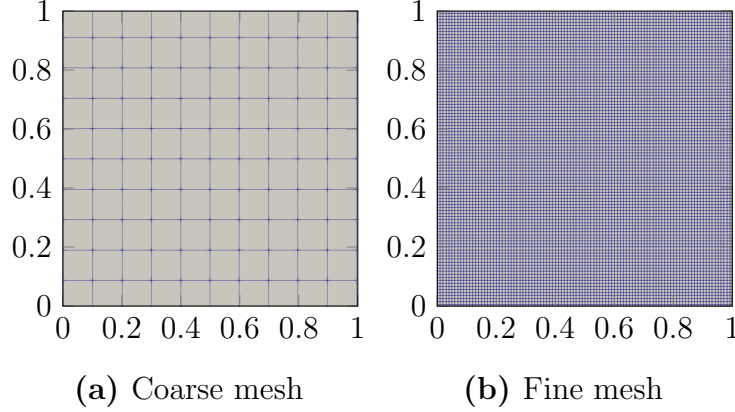


Figure 6: The low-resolution input mesh (10×10) and the high-resolution output mesh (200×200). The LR data will be refined by $400\times$

stationary Gaussian process,

$$f(\mathbf{x}) \sim \mathcal{GP}(\mathbf{0}, K(\mathbf{x}, \mathbf{x}')), \quad K(\mathbf{x}, \mathbf{x}') = \sigma^2 \exp\left(-\frac{|\mathbf{x} - \mathbf{x}'|^2}{2l^2}\right), \quad \text{in } \partial\Omega_{\text{inlet}} \quad (12)$$

where $K(\mathbf{x}, \mathbf{x}')$ is the exponential kernel function; l and σ represent the homogeneous length scale and standard deviation of the Gaussian random field. Here we set the length scale $l = 0.1$ and the standard deviation $\sigma = 0.33$. To represent the Gaussian process in a compact form, we use Karhunen-Loeve (KL) expansion,

$$f(\mathbf{x}) = \sum_{i=1}^{n_k \rightarrow \infty} \sqrt{\lambda_i} \phi_i(\mathbf{x}) \omega_i, \quad (13)$$

where λ and $\phi(\mathbf{x})$ are eigenvalues and eigenfunctions of the kernel, respectively; ω_i are uncorrelated random variables with zero mean and unit variance. We further truncate the KL expansion with a finite number ($n_k = 10$) of basis to capture 99.96% energy of the random field. The stream-wise velocity field (u) and the transverse velocity field (v) are defined as,

$$u(\mathbf{x}) = 1 + f(\mathbf{x}), \quad v(\mathbf{x}) = f(\mathbf{x}). \quad (14)$$

Hence, the inlet boundary condition is parameterized by a 20-dimensional parameter vector,

$$\boldsymbol{\mu} = [\omega_1, \dots, \omega_{20}]^T \in \mathbb{R}^{20}, \quad (15)$$

where $\omega_1, \dots, \omega_{10}$ parameterize the stream-wise velocity and $\omega_{11}, \dots, \omega_{20}$ are for the transverse velocity field. The first 10 KL modes are shown in the Fig. B.10.

The CNN-SR model is trained on 15 inlet samples randomly drawn from the Gaussian process defined by Eq. 12, where the PDE-based loss function is minimized with 10^3 iterations. Once the CNN-SR model is trained, it can super-resolve the LR flow fields of these 15 inlet samples and be used as a surrogate model to rapidly refine any LR data with unseen inlets in the 20-dimensional parameter space. To evaluate the model’s generalizability, we generate 985 new testing inlets that are unseen during the training. Figure 7 shows the CNN-SR results of 16 samples randomly selected from the test set, where noise-free LR data are used as the input. Though without any noise, the LR data contain very limited flow information because of the mesh coarseness (100×100). Both bicubic interpolation and trained CNN-SR model can spatially refine the LR data by $400\times$ and show improvements. However, the CNN-SR results reveal more flow details and have a better agreement with the HR reference.

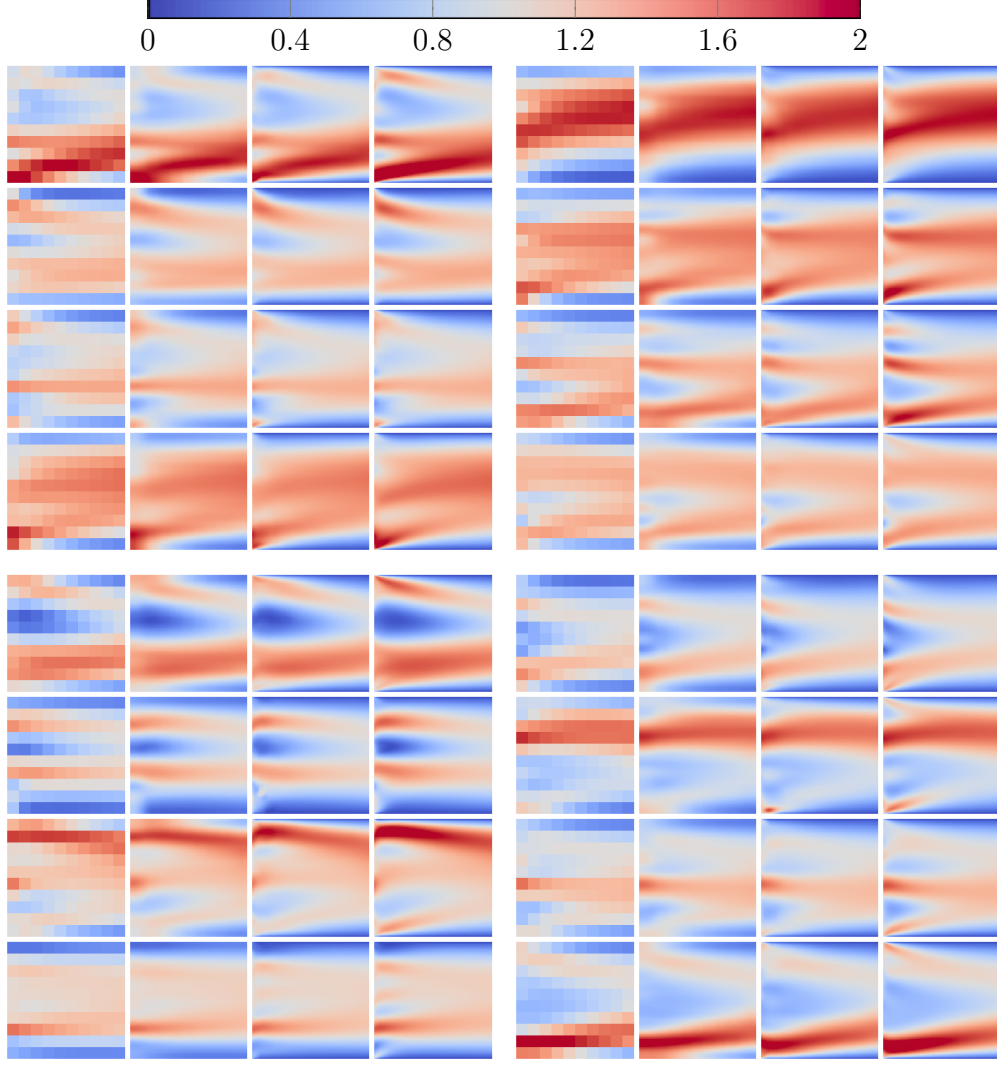


Figure 7: The CNN-SR results of noisy-free LR data on a subset of testing inlet samples randomly drawn from the Gaussian process. In every block, each row has a same inlet velocity field, and the LR data, bicubic-SR results, CNN-SR results, and HR reference are listed from the left to the right.

When the LR data contain noises, the superiority of the CNN-SR solution becomes more significant compared to the bicubic interpolation. To demonstrate this merit, we conduct another numerical experiment, where the LR data are corrupted with 20% Gaussian noise (noise level $c = 0.2$). The CNN-SR model is trained on the LR data by resampling the noise at every iteration to recognize the noisy inputs. Figure 8 shows the super-resolution results

of noisy LR data. It is apparent that the bicubic-SR velocity fields are visually unphysical by directly interpolating the data noises. The SR performance of the physics-informed CNN model still remains excellent as it accurately refined the spatial resolution of the LR data by $400\times$, and the SR results agree with the HR reference very well on all testing samples.

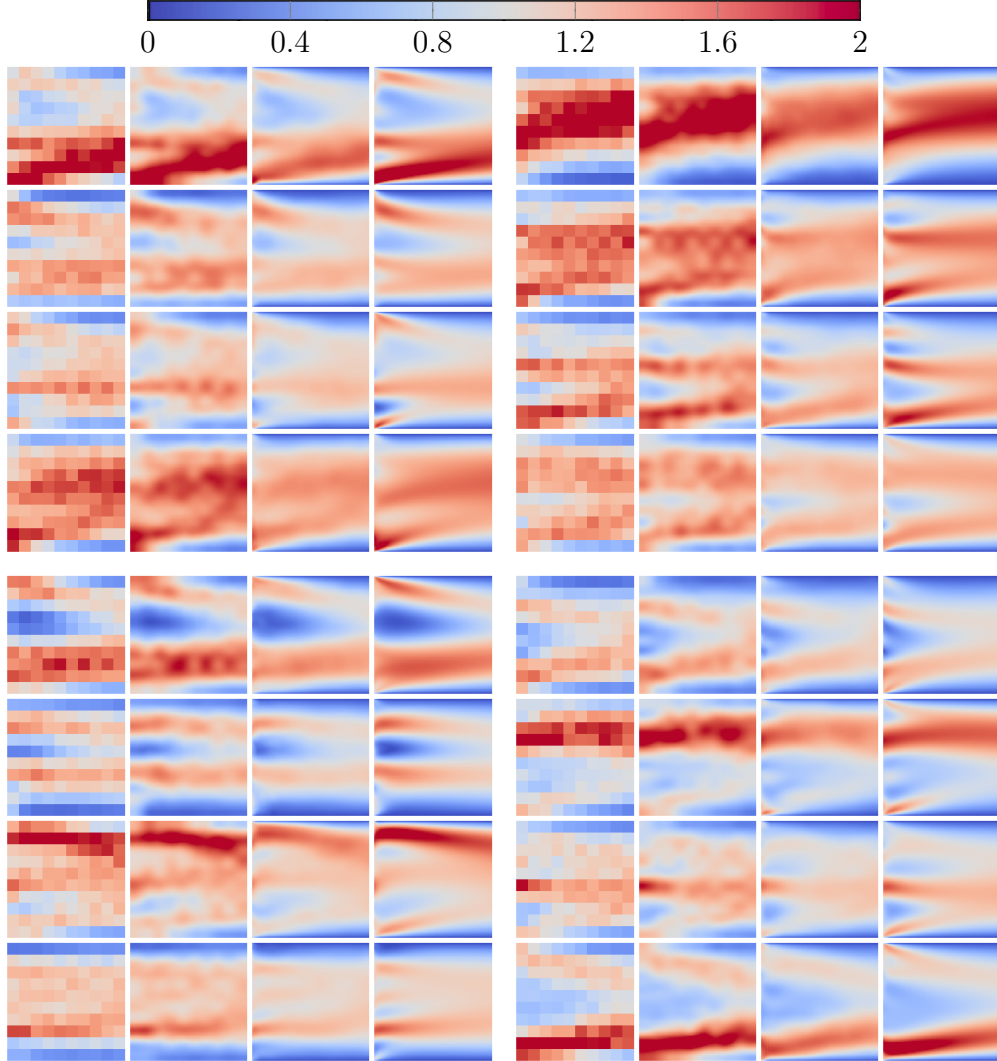


Figure 8: The CNN-SR results of noisy LR data on a subset of testing inlet samples randomly drawn from the Gaussian process. In every block, each row has a same inlet velocity field, and the LR data, bicubic-SR results, CNN-SR results, and HR reference are listed from the left to the right.

Figure 9 shows the mean relative errors versus LR data noise levels for both CNN-SR

and bicubic-SR results over 1000 testing samples. We can see the SR performance of bicubic interpolation remarkably deteriorates as the input noise level increases. When the LR data contain 100% noises, the naive bicubic interpolation completely fails as the relative error grows up to nearly 50%. In comparison, CNN-SR solutions are less sensitive to the growth of data noise. Although showing a similar trend, the CNN-SR solutions’ relative error remains small (less than 10%), even the data noise level reaches to 100%.

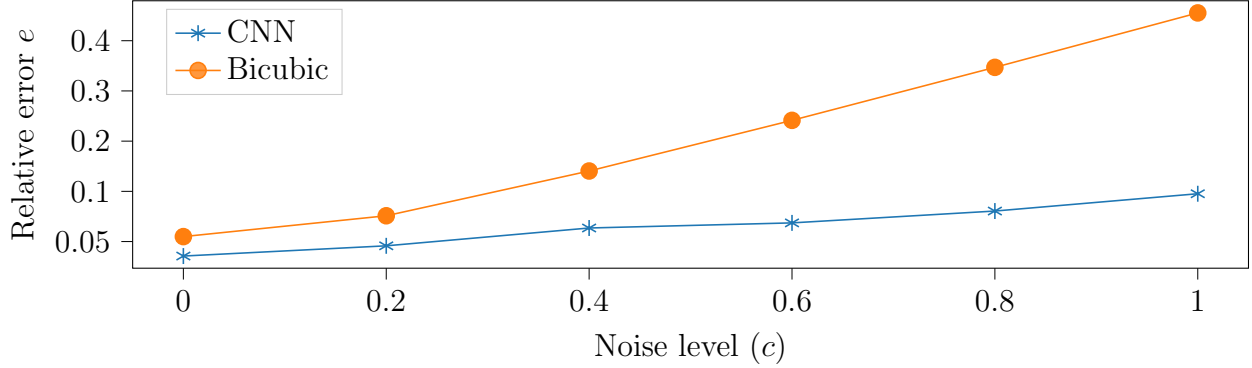


Figure 9: The relative errors of CNN and Bicubic SR results of LR inputs with different noise levels over 1000 testing samples.

The computational costs of a single model evaluation for the HR CFD and CNN-SR models are listed in Table 2. For a single run on each parameter point, the speedup of the CNN-SR model is more than 3000 times compared to the CFD simulation. It shows the potential of using the CNN-SR model as a surrogate for massive queries in the high-dimensional input space, which could enable or facilitate ensemble-based uncertainty quantification or inverse optimization.

	HR CFD	CNN
Wall-clock time (s)	4	1.189×10^{-3}
Hardware	Intel Xeon(R) Gold 6138	GeForce RTX 2080
Speedup	3364	

Table 2: Computational costs of online evaluation of the HR CFD and CNN-SR models.

4. Conclusion

In this paper, we proposed a novel physics-informed deep learning solution for the spatial super-resolution of flow fields. Leveraging the physical laws and boundary conditions of fluid flows, the training of the CNN-SR model only needs LR samples instead of its HR counterparts as labels. Once sufficiently trained, the CNN-SR model can produce the spatially refined flow field, given a noisy LR input in the parameter space. When the flow boundary conditions are unknown, the proposed framework can naturally assimilate additional sparse observation data to simultaneously enable forward SR and inverse determination of unknown boundary conditions. The effectiveness and merit of the proposed CNN-SR model have been demonstrated on a number of non-parametric and parametric spatial flow SR problems relevant to cardiovascular applications, where both Gaussian and non-Gaussian MRI noises are investigated. In particular, we demonstrated that the CNN-SR model, by training on only 15 LR input samples, is able to accurately refine the spatial resolution by $400\times$ for the flow fields with any new inlet BCs sampled in the 20-dimensional parameter space ($\boldsymbol{\mu} \in \mathbb{R}^{20}$). Compared to the standard SR approach based on the bicubic interpolation, the CNN-SR model shows significantly higher accuracy and robustness. Compared to the standard FV simulation, the single sample speedup is more than 10^3 times, showing its potential for many-query applications. The current work is only focused on the spatial super resolution for 2D flow fields. Future work will extend the framework for both spatial and temporal super-resolution of unsteady fluid flows in 3D complex domains.

Compliance with Ethical Standards

The authors declare that they have no conflict of interest.

Acknowledgement

The author gratefully acknowledge the funds from National Science Foundation (NSF contract: CMMI-1934300) in supporting this project.

Appendix A. Convolution operators for gradient and Laplacian terms

The convolution filters for gradient and laplacian terms are stored as 4D tensors shown as below,

$$\frac{\partial u}{\partial x} \text{ filter} = \left[\left[\left[\left[\begin{array}{ccccc} 0 & 0 & 0 & 0 & 0 \\ 0 & 0 & 0 & 0 & 0 \\ 1 & -8 & 0 & 8 & -1 \\ 0 & 0 & 0 & 0 & 0 \\ 0 & 0 & 0 & 0 & 0 \end{array} \right] \right] \right] \right] \times \frac{1}{12\delta x}, \quad (\text{A.1})$$

$$\frac{\partial u}{\partial y} \text{ filter} = \left[\left[\left[\left[\begin{array}{ccccc} 0 & 0 & 1 & 0 & 0 \\ 0 & 0 & -8 & 0 & 0 \\ 0 & 0 & 0 & 0 & 0 \\ 0 & 0 & 8 & 0 & 0 \\ 0 & 0 & -1 & 0 & 0 \end{array} \right] \right] \right] \right] \times \frac{1}{12\delta y}, \quad (\text{A.2})$$

and

$$\left(\frac{\partial^2 u}{\partial x^2} + \frac{\partial^2 u}{\partial y^2} \right) \text{ filter} = \left[\left[\left[\left[\begin{array}{ccccc} 0 & 0 & -1 & 0 & 0 \\ 0 & 0 & 16 & 0 & 0 \\ -1 & 16 & -60 & 16 & -1 \\ 0 & 0 & 16 & 0 & 0 \\ 0 & 0 & -1 & 0 & 0 \end{array} \right] \right] \right] \right] \times \frac{1}{12\delta x \delta y}, \quad \delta x = \delta y \quad (\text{A.3})$$

Appendix B. The KL modes for the spatially-varying inlets

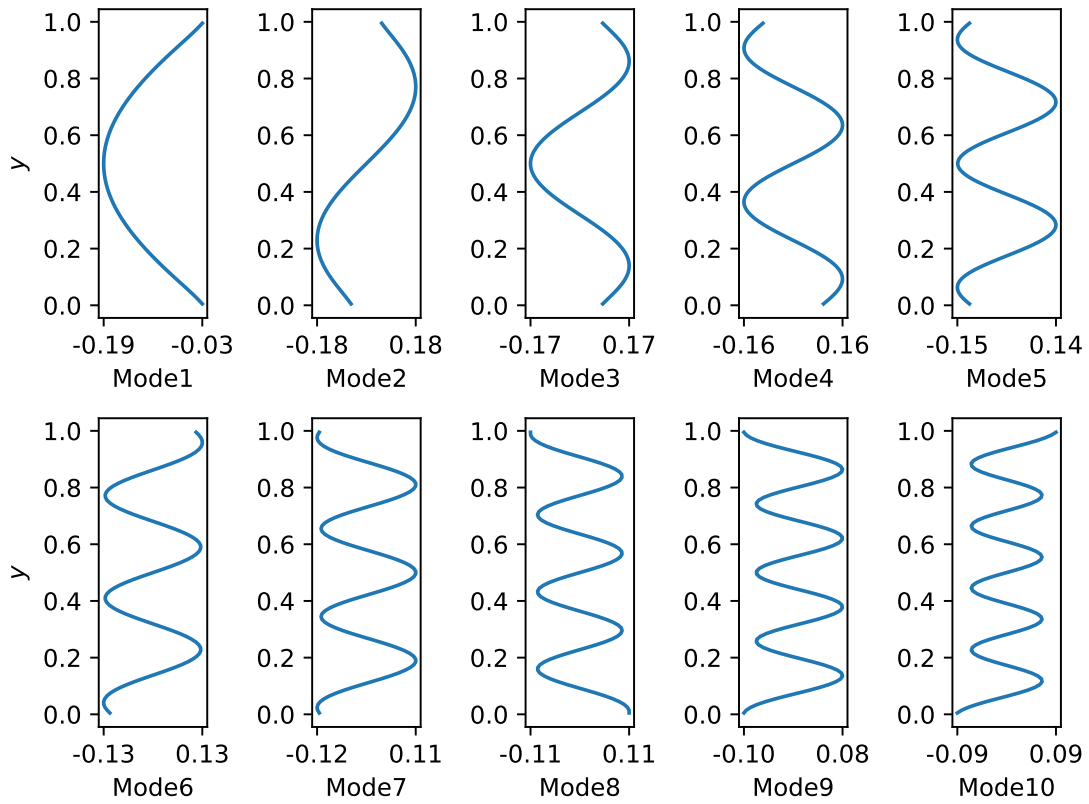


Figure B.10: The first 10 KL modes of the Gaussian random fields for the spatially-varying inlet boundary conditions.

Appendix C. Physics-informed training history

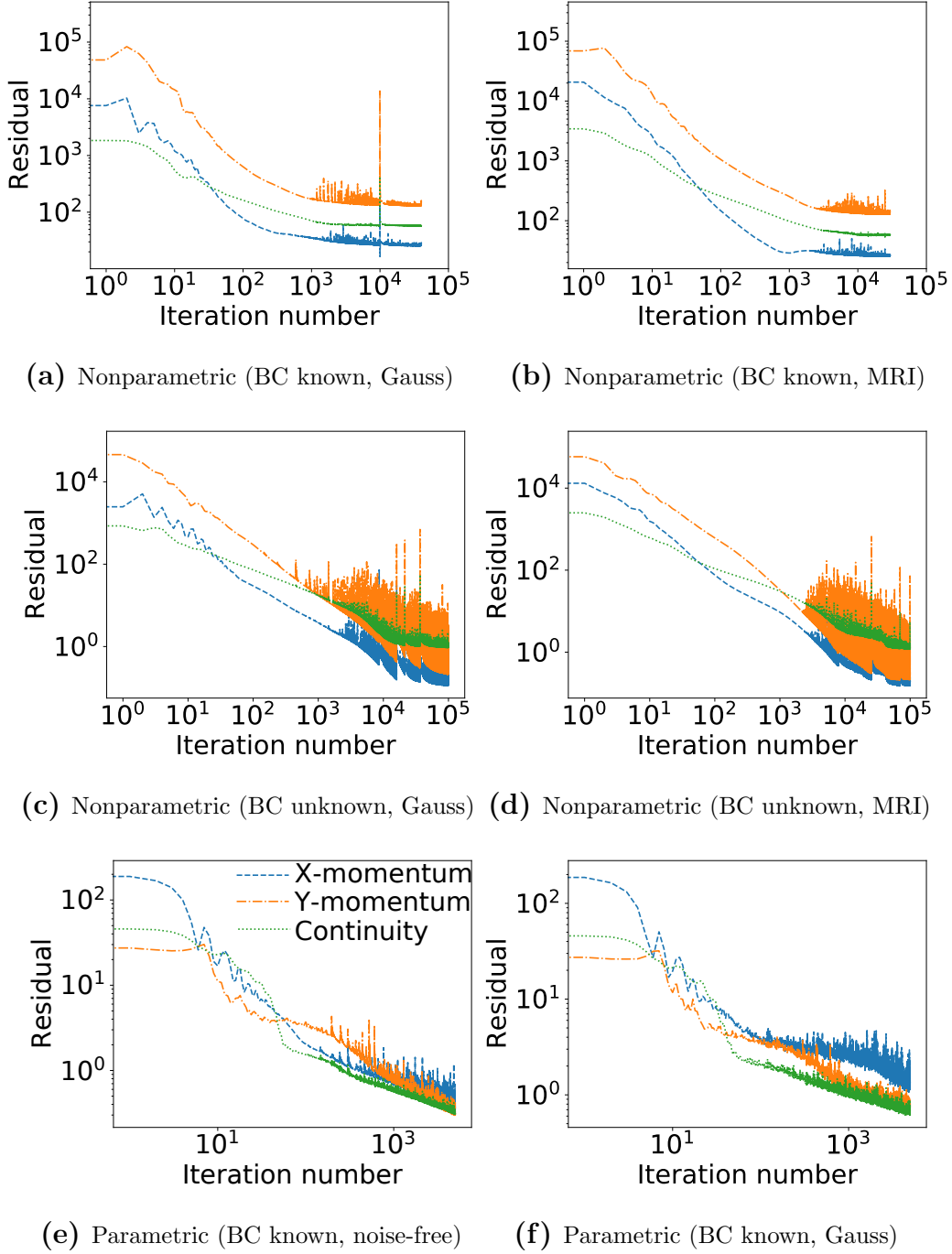


Figure C.11: Training histories for nonparametric and parametric super-resolution cases. Each iteration takes about 2 seconds on the NVIDIA 2080 GPU.

References

- [1] A. Pollard, L. Castillo, L. Danaila, M. Glauser, Whither turbulence and big data in the 21st century?, Springer, 2016.
- [2] C. M. Lawley, K. M. Broadhouse, F. M. Callaghan, D. S. Winlaw, G. A. Figtree, S. M. Grieve, 4d flow magnetic resonance imaging: role in pediatric congenital heart disease, *Asian Cardiovascular and Thoracic Annals* 26 (1) (2018) 28–37.
- [3] Z. Stankovic, B. D. Allen, J. Garcia, K. B. Jarvis, M. Markl, 4d flow imaging with mri, *Cardiovascular diagnosis and therapy* 4 (2) (2014) 173.
- [4] F. Ong, M. Uecker, U. Tariq, A. Hsiao, M. T. Alley, S. S. Vasanawala, M. Lustig, Robust 4d flow denoising using divergence-free wavelet transform, *Magnetic resonance in medicine* 73 (2) (2015) 828–842.
- [5] M. F. Fathi, A. Bakhshinejad, A. Baghaie, D. Saloner, R. H. Sacho, V. L. Rayz, R. M. D’Souza, Denoising and Spatial Resolution Enhancement of 4D Flow MRI Using Proper Orthogonal Decomposition and Lasso Regularization, *Computerized Medical Imaging and Graphics* 70 (2018) 1–20.
- [6] F. M. Callaghan, S. M. Grieve, Spatial resolution and velocity field improvement of 4D-flow MRI, *Magnetic Resonance in Medicine* 78 (5) (2017) 1959–1968.
- [7] D. Venturi, G. E. Karniadakis, Gappy data and reconstruction procedures for flow past a cylinder, *Journal of Fluid Mechanics* 519 (2004) 315–336.
- [8] T. Bui-Thanh, M. Damodaran, K. Willcox, Proper orthogonal decomposition extensions for parametric applications in compressible aerodynamics, in: *21st AIAA Applied Aerodynamics Conference*, 2003, p. 4213.
- [9] B. Podvin, Y. Fraigneau, F. Lusseyran, P. Gougat, A reconstruction method for the flow past an open cavity, *Journal of fluids engineering* 128 (3) (2006) 531–540.

- [10] A. Yakhot, T. Anor, G. E. Karniadakis, A reconstruction method for gappy and noisy arterial flow data, *IEEE transactions on medical imaging* 26 (12) (2007) 1681–1697.
- [11] A. I. Moreno, A. A. Jarzabek, J. M. Perales, J. M. Vega, Aerodynamic database reconstruction via gappy high order singular value decomposition, *Aerospace Science and Technology* 52 (2016) 115–128.
- [12] M. Mifsud, A. Vendl, L.-U. Hansen, S. Görtz, Fusing wind-tunnel measurements and cfd data using constrained gappy proper orthogonal decomposition, *Aerospace Science and Technology* 86 (2019) 312–326.
- [13] P. J. Schmid, Dynamic mode decomposition of numerical and experimental data, *Journal of fluid mechanics* 656 (2010) 5–28.
- [14] J. H. Tu, C. W. Rowley, D. M. Luchtenburg, S. L. Brunton, J. N. Kutz”, On dynamic mode decomposition: Theory and applications, *Journal of Computational Dynamics* 1 (2014) 391.
- [15] J. L. Callaham, K. Maeda, S. L. Brunton, Robust flow reconstruction from limited measurements via sparse representation, *Physical Review Fluids* 4 (10) (2019) 103907.
- [16] K. Manohar, B. W. Brunton, J. N. Kutz, S. L. Brunton, Data-driven sparse sensor placement for reconstruction: Demonstrating the benefits of exploiting known patterns, *IEEE Control Systems Magazine* 38 (3) (2018) 63–86.
- [17] D. P. Foures, N. Dovetta, D. Sipp, P. J. Schmid, A data-assimilation method for Reynolds-averaged Navier–Stokes-driven mean flow reconstruction, *Journal of Fluid Mechanics* 759 (2014) 404–431.
- [18] B. Combès, D. Heitz, A. Guibert, E. Mémin, A particle filter to reconstruct a free-surface flow from a depth camera, *Fluid Dynamics Research* 47 (5) (2015) 051404.

- [19] R. Kikuchi, T. Misaka, S. Obayashi, Assessment of probability density function based on POD reduced-order model for ensemble-based data assimilation, *Fluid Dynamics Research* 47 (5) (2015) 051403.
- [20] V. Mons, J.-C. Chassaing, T. Gomez, P. Sagaut, Reconstruction of unsteady viscous flows using data assimilation schemes, *Journal of Computational Physics* 316 (2016) 255–280.
- [21] S. Symon, N. Dovetta, B. J. McKeon, D. Sipp, P. J. Schmid, Data assimilation of mean velocity from 2d piv measurements of flow over an idealized airfoil, *Experiments in fluids* 58 (5) (2017) 61.
- [22] J.-X. Wang, H. Xiao, Data-driven cfd modeling of turbulent flows through complex structures, *International Journal of Heat and Fluid Flow* 62 (2016) 138–149.
- [23] H. Xiao, J.-L. Wu, J.-X. Wang, R. Sun, C. Roy, Quantifying and reducing model-form uncertainties in reynolds-averaged navier–stokes simulations: A data-driven, physics-informed bayesian approach, *Journal of Computational Physics* 324 (2016) 115–136.
- [24] S. L. Brunton, B. R. Noack, P. Koumoutsakos, Machine learning for fluid mechanics, *Annual Review of Fluid Mechanics* 52 (2020) 477–508.
- [25] M. Brenner, J. Eldredge, J. Freund, Perspective on machine learning for advancing fluid mechanics, *Physical Review Fluids* 4 (10) (2019) 100501.
- [26] J. Ling, A. Kurzawski, J. Templeton, Reynolds averaged turbulence modelling using deep neural networks with embedded invariance, *Journal of Fluid Mechanics* 807 (2016) 155–166.
- [27] K. Duraisamy, G. Iaccarino, H. Xiao, Turbulence modeling in the age of data, *Annual Review of Fluid Mechanics* 51 (2019) 357–377.

- [28] J.-X. Wang, J.-L. Wu, H. Xiao, Physics-informed machine learning approach for reconstructing reynolds stress modeling discrepancies based on dns data, *Physical Review Fluids* 2 (3) (2017) 034603.
- [29] J.-X. Wang, J. Huang, L. Duan, H. Xiao, Prediction of reynolds stresses in high-mach-number turbulent boundary layers using physics-informed machine learning, *Theoretical and Computational Fluid Dynamics* 33 (1) (2019) 1–19.
- [30] M. I. Zafar, H. Xiao, M. M. Choudhari, F. Li, C.-L. Chang, P. Paredes, B. Venkatachari, Convolutional neural network for transition modeling based on linear stability theory, *arXiv preprint arXiv:2005.02599*.
- [31] K. Fukami, Y. Nabae, K. Kawai, K. Fukagata, Synthetic turbulent inflow generator using machine learning, *Physical Review Fluids* 4 (6) (2019) 064603.
- [32] J. Kim, C. Lee, Deep unsupervised learning of turbulence for inflow generation at various reynolds numbers, *Journal of Computational Physics* 406 (2020) 109216.
- [33] L. Sun, H. Gao, S. Pan, J.-X. Wang, Surrogate modeling for fluid flows based on physics-constrained deep learning without simulation data, *Computer Methods in Applied Mechanics and Engineering* 361 (2020) 112732.
- [34] R. Maulik, K. Fukami, N. Ramachandra, K. Fukagata, K. Taira, Probabilistic neural networks for fluid flow surrogate modeling and data recovery, *Physical Review Fluids* 5 (10) (2020) 104401.
- [35] H. Gao, J.-X. Wang, M. J. Zahr, Non-intrusive model reduction of large-scale, nonlinear dynamical systems using deep learning, *arXiv preprint arXiv:1911.03808*.
- [36] C. Ledig, L. Theis, F. Huszár, J. Caballero, A. Cunningham, A. Acosta, A. Aitken, A. Tejani, J. Totz, Z. Wang, et al., Photo-realistic single image super-resolution using a generative adversarial network, in: *Proceedings of the IEEE conference on computer vision and pattern recognition*, 2017, pp. 4681–4690.

- [37] K. Fukami, K. Fukagata, K. Taira, Machine learning based spatio-temporal super resolution reconstruction of turbulent flows, arXiv preprint arXiv:2004.11566.
- [38] K. Fukami, K. Fukagata, K. Taira, Super-resolution analysis with machine learning for low-resolution flow data, in: 11th International Symposium on Turbulence and Shear Flow Phenomena, TSFP 2019, 2019.
- [39] K. Fukami, K. Fukagata, K. Taira, Super-resolution reconstruction of turbulent flows with machine learning, arXiv preprint arXiv:1811.11328.
- [40] Y. Liu, C. Ponce, S. L. Brunton, J. N. Kutz, Multiresolution convolutional autoencoders, arXiv preprint arXiv:2004.04946.
- [41] Z. Deng, C. He, Y. Liu, K. C. Kim, Super-resolution reconstruction of turbulent velocity fields using a generative adversarial network-based artificial intelligence framework, *Physics of Fluids* 31 (12) (2019) 125111.
- [42] M. Bode, M. Gauding, Z. Lian, D. Denker, M. Davidovic, K. Kleinheinz, J. Jitsev, H. Pitsch, Using physics-informed super-resolution generative adversarial networks for subgrid modeling in turbulent reactive flows, arXiv preprint arXiv:1911.11380.
- [43] K. Bai, W. Li, M. Desbrun, X. Liu, Dynamic upsampling of smoke through dictionary-based learning, arXiv preprint arXiv:1910.09166.
- [44] F. J. Gonzalez, M. Balajewicz, Deep convolutional recurrent autoencoders for learning low-dimensional feature dynamics of fluid systems, arXiv preprint arXiv:1808.01346.
- [45] Y. Xie, E. Franz, M. Chu, N. Thuerey, tempogan: A temporally coherent, volumetric gan for super-resolution fluid flow, *ACM Transactions on Graphics (TOG)* 37 (4) (2018) 1–15.
- [46] B. Liu, J. Tang, H. Huang, X.-Y. Lu, Deep learning methods for super-resolution reconstruction of turbulent flows, *Physics of Fluids* 32 (2) (2020) 025105.

- [47] M. Werhahn, Y. Xie, M. Chu, N. Thuerey, A multi-pass gan for fluid flow super-resolution, *Proceedings of the ACM on Computer Graphics and Interactive Techniques* 2 (2) (2019) 1–21.
- [48] L. Guo, S. Ye, J. Han, H. Zheng, H. Gao, D. Z. Chen, J.-X. Wang, C. Wang, Ssr-vfd: Spatial super-resolution for vector field data analysis and visualization, in: *2020 IEEE Pacific Visualization Symposium (PacificVis)*, IEEE, 2020, pp. 71–80.
- [49] N. B. Erichson, L. Mathelin, Z. Yao, S. L. Brunton, M. W. Mahoney, J. N. Kutz, Shallow learning for fluid flow reconstruction with limited sensors and limited data, *arXiv preprint arXiv:1902.07358*.
- [50] E. Ferdian, A. Suinesiaputra, D. J. Dubowitz, D. Zhao, A. Wang, B. Cowan, A. A. Young, 4DFlowNet: Super-resolution 4d flow MRI using deep learning and computational fluid dynamics, *Frontiers in Physics* 8 (2020) 138.
- [51] M. Raissi, P. Perdikaris, G. Karniadakis, Physics-informed neural networks: A deep learning framework for solving forward and inverse problems involving nonlinear partial differential equations, *Journal of Computational Physics* 378 (2019) 686–707.
- [52] V. Dwivedi, N. Parashar, B. Srinivasan, Distributed learning machines for solving forward and inverse problems in partial differential equations, *Neurocomputing* 420 299–316.
- [53] Y. Zhu, N. Zabaras, P.-S. Koutsourelakis, P. Perdikaris, Physics-constrained deep learning for high-dimensional surrogate modeling and uncertainty quantification without labeled data, *Journal of Computational Physics* 394 (2019) 56–81.
- [54] N. Geneva, N. Zabaras, [Modeling the dynamics of PDE systems with physics-constrained deep auto-regressive networks](#), *Journal of Computational Physics* 403 (2020) 109056. doi:10.1016/j.jcp.2019.109056.
URL <https://linkinghub.elsevier.com/retrieve/pii/S0021999119307612>

- [55] R. Zhang, Y. Liu, H. Sun, Physics-informed multi-lstm networks for metamodeling of nonlinear structures, arXiv preprint arXiv:2002.10253.
- [56] Z. Long, Y. Lu, X. Ma, B. Dong, PDE-net: Learning PDEs from data, arXiv preprint arXiv:1710.09668.
- [57] Z. Long, Y. Lu, B. Dong, PDE-Net 2.0: Learning PDEs from data with a numeric-symbolic hybrid deep network, *Journal of Computational Physics* 399 (2019) 108925.
- [58] G. Singh, S. Gupta, M. Lease, C. N. Dawson, TIME: A transparent, interpretable, model-adaptive and explainable neural network for dynamic physical processes, arXiv preprint arXiv:2003.02426.
- [59] Z. Chen, Y. Liu, H. Sun, Deep learning of physical laws from scarce data, arXiv preprint arXiv:2005.03448.
- [60] C. M. Jiang, S. Esmailzadeh, K. Azizzadenesheli, K. Kashinath, M. Mustafa, H. A. Tchelepi, P. Marcus, A. Anandkumar, et al., Meshfreeflownet: A physics-constrained deep continuous space-time super-resolution framework, arXiv preprint arXiv:2005.01463.
- [61] A. T. Mohan, N. Lubbers, D. Livescu, M. Chertkov, Embedding hard physical constraints in neural network coarse-graining of 3d turbulence, arXiv preprint arXiv:2002.00021.
- [62] N. Thuerey, Y. Xie, M. Chu, S. Wiewel, L. Prantl, Physics-based deep learning for fluid flow.
- [63] A. Subramaniam, M. L. Wong, R. D. Borker, S. Nimmagadda, S. K. Lele, Turbulence enrichment using physics-informed generative adversarial networks, arXiv (2020) arXiv:2003.2003.
- [64] L. Sun, J.-X. Wang, Physics-constrained bayesian neural network for fluid flow reconstruction with sparse and noisy data, arXiv preprint arXiv:2001.05542.

- [65] L. Sun, H. Gao, S. Pan, J.-X. Wang, Surrogate modeling for fluid flows based on physics-constrained deep learning without simulation data, *Computer Methods in Applied Mechanics and Engineering* doi:<https://doi.org/10.1016/j.cma.2019.112732>.
- [66] H. Gao, L. Sun, J.-X. Wang, Phygeonet: Physics-informed geometry-adaptive convolutional neural networks for solving parametric pdes on irregular domain, *arXiv preprint arXiv:2004.13145*.
- [67] W. Shi, J. Caballero, F. Huszár, J. Totz, A. P. Aitken, R. Bishop, D. Rueckert, Z. Wang, Real-time single image and video super-resolution using an efficient sub-pixel convolutional neural network, in: *Proceedings of the IEEE conference on computer vision and pattern recognition*, 2016, pp. 1874–1883.
- [68] D. P. Kingma, J. Ba, Adam: A method for stochastic optimization, *arXiv preprint arXiv:1412.6980*.
- [69] V. Nair, G. E. Hinton, Rectified linear units improve restricted boltzmann machines, in: *ICML*, 2010.
- [70] K. M. Johnson, M. Markl, Improved snr in phase contrast velocimetry with five-point balanced flow encoding, *Magnetic Resonance in Medicine: An Official Journal of the International Society for Magnetic Resonance in Medicine* 63 (2) (2010) 349–355.
- [71] H. Jasak, A. Jemcov, Z. Tukovic, et al., Openfoam: A c++ library for complex physics simulations, in: *International workshop on coupled methods in numerical dynamics*, Vol. 1000, IUC Dubrovnik Croatia, 2007, pp. 1–20.
- [72] R. H. Pletcher, J. C. Tannehill, D. Anderson, *Computational fluid mechanics and heat transfer*, CRC press, 2012.
- [73] C. Rhie, W. L. Chow, Numerical study of the turbulent flow past an airfoil with trailing edge separation, *AIAA journal* 21 (11) (1983) 1525–1532.

- [74] A. Paszke, S. Gross, S. Chintala, G. Chanan, E. Yang, Z. DeVito, Z. Lin, A. Desmaison, L. Antiga, A. Lerer, Automatic differentiation in pytorch.